TISSUE ENGINEERING: Part A
Volume 25, Numbers 23 and 24, 2019

DOI: 10.1089/ten.tea.2018.0319

termis
Tissue Engineering
& Regenerative Medicine
International Society

ORIGINAL ARTICLE

Core–Shell Nanofibrous Scaffolds for Repair of Meniscus Tears

Jihye Baek, PhD,[1,2] Martin K. Lotz, MD,[2] and Darryl D. D'Lima, MD, PhD[1,2]

Electrospinning is an attractive method of fabricating nanofibers that replicate the ultrastructure of the human meniscus. However, it is challenging to approximate the mechanical properties of meniscal tissue while maintaining the biocompatibility of collagen fibers. Our objective was to determine if functionalizing polylactic acid (PLA) nanofibers with collagen would enhance their biocompatibility. We therefore used coaxial electrospinning to generate core–shell nanofibers with a core of PLA for mechanical strength and a shell of collagen to enhance cell attachment and matrix synthesis. We characterized the nanostructure of the engineered scaffolds and measured the hydrophilic and mechanical properties. We assessed the performance of human meniscal cells seeded on coaxial electrospun scaffolds to produce meniscal tissue by gene expression and histology. Finally, we investigated whether these cell-seeded scaffolds could repair surgical tears created *ex vivo* in avascular meniscal explants. Histology, immunohistochemistry, and mechanical testing of *ex vivo* repair provided evidence of neotissue that was significantly better integrated with the native tissue than with the acellular coaxial electrospun scaffolds. Human meniscal cell-seeded coaxial electrospun scaffolds may have potential in enhancing repair of avascular meniscus tears.

Keywords: coaxial electrospinning, core–shell structure, nanofibers, tissue engineering

Impact Statement

The success of any tissue-engineered meniscus graft relies on its ability to mimic native three-dimensional microstructure, support cell growth, produce tissue-specific matrix, and enhance graft integration into the repair site. Polylactic acid scaffolds possess the desired mechanical properties, whereas collagen scaffolds induce better cell attachment and enhanced tissue regeneration. We therefore fabricated nanofibrous scaffolds that combined the properties of two biomaterials. These novel coaxial scaffolds more closely emulated the structure, mechanical properties, and biochemical composition of native meniscal tissue. Our findings of meniscogenic tissue generation and integration in meniscus defects have the potential to be translated to clinical use.

Introduction

The meniscus plays an important biomechanical role in the knee; meniscal tears or degeneration are often associated with progressive arthritis.[1] Surgery for meniscal tears or degeneration is the most common orthopedic operation.[2] Repair of a meniscal tear in the vascular region is sometimes successful, but repair of tears in the avascular region is unlikely because of the lack of blood supply.[3] Consequently, there is a significant unmet need for the repair and restoration of meniscus function after injury or degeneration.[4] Cell-based tissue engineering is an attractive approach to recapitulate the structure and function of the tissue.[5] The regeneration of damaged or lost dense connective tissues, such as the meniscus, requires that regenerative cells assemble three dimensionally in and around an appropriately structured supporting scaffold.[6] An ideal scaffold should be biocompatible and biodegradable, possess the appropriate biomechanical properties, and facilitate surgical handling for secure implantation. The quality of the tissue-engineered construct is initially determined by the structure and biochemical composition of the supporting matrix where the cells are cultured. The performance of the cells in the scaffolds and their meniscogenic response determines the long-term function after implantation.

The biomechanical anisotropy of the meniscus is predominantly determined by fibrous structures with individual fiber size ranging from the nanometer to millimeter scale.[7]

[1]Shiley Center for Orthopedic Research and Education, Scripps Clinic, La Jolla, California.
[2]Department of Molecular Medicine, The Scripps Research Institute, La Jolla, California.

Therefore, nanofibrous scaffolds have been fabricated and have been analyzed to mimic these natural matrices. We previously demonstrated that electrospinning polylactic acid (PLA) and collagen could replicate meniscus nanostructural and microstructural organization with promising mechanical properties and cell compatibility.[8,9] Collagen scaffolds were significantly more biocompatible than PLA scaffolds and enhanced cell attachment and proliferation. Despite the attractive biocompatibility of collagen scaffolds, hydration significantly reduced mechanical properties,[9,10] which also compromised feasibility for surgical handling and biomechanical performance after implantation.[11] On the other hand, PLA scaffolds were stiffer and their mechanical properties better approximated those of native human meniscus. We therefore sought to combine the biomechanical strengths of PLA with the biocompatible advantages of collagen.

One study electrospun layers of PLA, polycaprolactone (PCL), and collagen into a membrane for dural repair, but only one side of the membrane contained collagen.[12] Another study electrospun an emulsion of PLA and collagen in a monofilament for antibiotic release, but the relative distribution of collagen versus PLA within the fibers could not be controlled.[13] Mixing collagen with PLA reduces the strength of PLA and the biocompatibility of collagen and results in a hydrophobic polymer surface.

One approach to combine the properties of synthetic and natural polymers is to generate core–shell structures. Approaches for generating core–shell nanofibers include coaxial electrospinning,[14,15] emulsion electrospinning,[16,17] template deposition,[18,19] electrostatic force induction,[20] phase separation,[21] and other techniques.[22–24] Coaxial electrospinning is a modification of traditional electrospinning in which the single spinneret is replaced with two coaxial capillaries, the channels of which are connected to two separate reservoirs. The coaxial configuration of nozzles provides independent pathways for the inner and outer solutions that generate a jet of fluid containing a core of the inner solution encased in a shell of the outer solution. The coaxial electrospinning configuration is illustrated in Figure 1A and the coaxial nozzle shown in Figure 1B.

We hypothesized that coaxial electrospun scaffolds containing a core of PLA and a shell of collagen I possess mechanical properties approaching that of native meniscal tissue, upregulate the expression of meniscogenic genes, induce the secretion of fibrocartilaginous extracellular matrix, and promote integration into meniscal tears. To test these hypotheses, we electrospun core–shell scaffolds composed of a core of PLA and a shell of collagen I. We characterized fiber morphology, biomechanical properties, cell viability and proliferation, gene expression, and matrix synthesis. To determine potential for clinical translation, we also evaluated *ex vivo* repair by implanting cell-seeded coaxial electrospun scaffolds in tears created in the avascular region of live bovine meniscal explants.

Materials and Methods

Fabrication of electrospun scaffolds

An overview of the coaxial system used to generate scaffolds is shown in Figure 1A. PLA (5% w/v, Mw = 100,000; NatureWorks, MN) and collagen type I (10% w/v, Semed S, acid-soluble; DSM, NL) solutions were prepared by dissolving in 1,1,1,3,3,3-hexafluoro-2-propanol (HFIP; Chem-Impex International, Inc., IL). A dual concentric nozzle (NNC-30kV-2mA portable type; NanoNC, South Korea) (Fig. 1B) was used for coaxial electrospinning to generate fibers with a core of PLA and a shell of collagen. The PLA and collagen solutions were placed in different syringes, which were individually actuated by syringe pumps (KDS200; KD Scientific, Inc., MA) at a feed rate of 1–2 mL h^{-1}. The coaxial scaffolds were electrospun on a drum cylinder rotating at 2400 rpm to generate aligned fibers. The applied voltage was adjusted between 15 and 20 kV using a voltage regulator DC power supply (NNC-30kV-2mA portable type; NanoNC, South Korea) to induce a polymer jet. For comparison, PLA-only and collagen-only mats were also independently electrospun. To stabilize the electrospun collagen, scaffolds were crosslinked in 0.25% glutaraldehyde (Sigma-Aldrich, St. Louis, MO) in absolute ethanol for 1 h. After crosslinking, scaffolds were washed three times for 10 min each with absolute ethanol and were stored at 4°C.

Characterization of scaffolds

The electrospun scaffolds were coated with iridium using a sputter coater (Emitech K575X; EM Technologies Ltd., England) for scanning electron microscopy (SEM, Philips XL30; FEI Co., Hillsboro, OR) with an accelerating voltage of 10 kV. The diameter of the electrospun fibers was measured from the SEM images using image-processing software (ImageJ; National Institutes of Health, Bethesda, MD). The core–shell structure of the coaxial electrospun nanofibers was examined by transmission electron microscopy (TEM, FEI Tecnai 12 Spirit; FEI Co., Hillsboro, OR). The samples for TEM were prepared by directly depositing the as-spun nanofibers onto a copper grid on a flat plate as a collector. The samples were dried in a vacuum oven at room temperature for 48 h before the TEM imaging. The TEM machine was operated at 120 kV Fourier transform infrared (FTIR) spectroscopy (PerkinElmer FTIR; PerkinElmer, Waltham, MA) was carried out to detect any chemical changes among three different scaffolds, PLA, collagen, and coaxial electrospun scaffolds. Thermogravimetric analysis (TGA) was carried out with a PerkinElmer Pyris 1 TGA (PerkinElmer, Waltham, MA) at a scan rate of 10°C/min under inert atmosphere with PLA, collagen, and coaxial electrospun scaffolds.

Hydrophilic properties of scaffolds

The contact angle of a water droplet was measured as previously described.[8,9] Each scaffold ($n = 7$ per scaffold type) was photographed with a digital camera with the lens positioned parallel to and centered on the scaffold. Image analysis was used to construct a line tangent to the surface of the water droplet and was used to measure the angle relative to the scaffold surface.

The water content of hydrated scaffolds was measured as previously described.[8,9] Each scaffold ($n = 6$ per group) was immersed in distilled water for 24 h at room temperature. The wet weight of the scaffolds (W_{wet}) was measured after removing excess water from the scaffolds. The scaffolds were then dried in an oven at 65°C overnight and the weight of dried scaffolds (W_{dry}) was measured. The water content was calculated as a percentage of the wet weight:

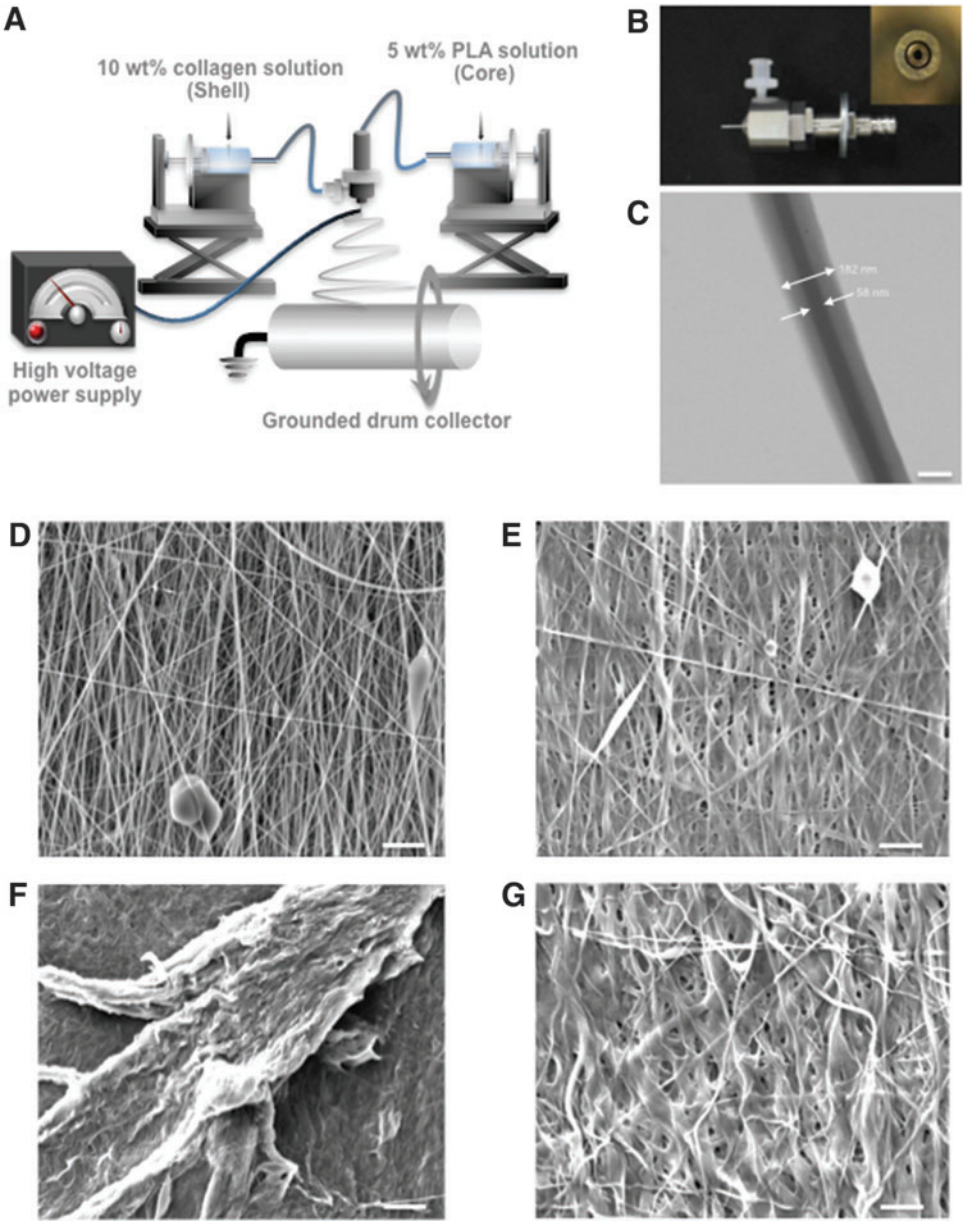

FIG. 1. Overview of coaxial electrospinning. **(A)** A rotating drum collector was used to deposit aligned electrospun fibers; **(B)** Photographs of the coaxial nozzle and cross-section of coaxial nozzle tip (*inset*). **(C)** TEM image of an individual coaxial nanofiber with a core of PLA and a shell of collagen (Mag.: 26,000×; scale bar: 100 nm). SEM (Mag.: 2500×; scale bar: 5 μm) of **(D)** noncrosslinked coaxial fibers; **(E)** crosslinked coaxial fibers with glutaraldehyde; **(F)** noncrosslinked coaxial fibers and **(G)** crosslinked coaxial fibers after 2 h exposure to culture medium at incubator. Mag., magnification; PLA, polylactic acid; SEM, scanning electron microscopy; TEM, transmission electron microscopy. Color images are available online.

Tissue harvesting and cell isolation

With Scripps Institutional Review Board approval, normal human menisci were obtained from tissue banks from six donors (mean age, 25.2 ± 9.84; age range, 19–35 years; two females and four males). A macroscopic and histological grading system was used to select normal menisci.[25] The avascular region, which comprises the inner two-thirds of each meniscus, was harvested and enzymatically digested using collagenase (2 mg mL^{-1}, C5138; Sigma-Aldrich) in DMEM (Mediatech, Inc., Manassas, VA) and 1% Penicillin-Streptomycin-Fungizone (Life Technologies, Carlsbad, CA) for 5 to 6 h. The digested tissues were filtered through 100 μm cell strainers (BD Biosciences, San Jose, CA) and cells were seeded in monolayer culture in DMEM (Mediatech) supplemented with 10% calf serum (Omega Scientific, Inc., Tarzana, CA) and 1% Penicillin–Streptomycin–Glutamine (Life Technologies). The freshly isolated meniscal cells were cultured for one passage before being seeded onto electrospun scaffolds.

Cell seeding in scaffolds

Human meniscus cells were seeded onto 2 × 1 cm rectangular scaffolds at a cell density of 0.5×10^6 per scaffold. Cell-seeded scaffolds were cultured in six-well plates and were maintained in 2 mL of DMEM (Mediatech) supplemented with 10% calf serum (Omega Scientific, Inc., Tarzana, CA) and 1% Penicillin–Streptomycin–Glutamine (Life Technologies) for 3 days, for initial cell attachment and scaffold colonization. The culture medium was then changed to serum-free ITS+ medium (Sigma) supplemented with 10 ng mL^{-1} TGFβ1 (PeproTech, Rocky Hill, NJ), or with no growth factor (control group) with subsequent medium changes every 3 to 4 days for 2 weeks.

Cellular morphology SEM

Cell-seeded scaffolds with either chemical crosslinking or no crosslinking were washed with 1×phosphate-buffered saline (PBS) and fixed with 2.5% w/v glutaraldehyde (Sigma-Aldrich) in 1×PBS for 1 h. After fixation, specimens were washed three times with PBS for 10 min each wash. Then the specimens were dehydrated in a graded series of ethanol (50%, 70%, and 90%) for 30 min each and were left in 100% ethanol for 24 h at temperatures below zero. Next, the specimens were kept in 100% ethanol until they were completely dried in a critical point dryer (Autosamdri-815, Series A; tousimis, Inc., Rockville, MD). The surface of dried samples was then metalized by sputter coating with iridium. The morphology of the scaffolds as well as that of the adherent cells was observed by SEM (Philips XL30).

Cell viability

The viability of cells cultured on the noncrosslinked and crosslinked scaffolds for 2 weeks was measured using Calcein-AM and Ethidium Homodimer-1 (Live/Dead Kit; Life Technologies) and using a laser confocal microscope (Zeiss LSM-510; Zeiss, Jena, Germany) as previously described.[26]

Scaffold mechanical properties

Tensile testing was performed as described previously.[9] Each scaffold type was tested under three different conditions: (1) dry scaffolds, (2) scaffolds without cells (acellular) and cultured for 2 weeks, and (3) scaffolds seeded with avascular human meniscus cells and cultured for 2 weeks. Scaffolds were cut into dog bone-shaped specimens with a gauge length of 8 mm and gauge width of 2 mm using a custom aluminum die cutter. The thickness of each scaffold was measured using a digital caliper.

Test specimens ($n=8$ per group) were mounted in the grips of a uniaxial testing machine (Instron® Universal Testing Machine; 3342 Single Column Model; Instron, Norwood, MA) with a 500 N load cell and were tested to failure at a displacement rate of 1 mm s^{-1}. The tensile modulus was calculated as the slope of the linear portion of the stress–strain curve. The maximum load before failure was used to calculate the ultimate tensile strength (UTS).

Measurement of newly deposited collagen type I

Human meniscal avascular cells were cultured on discs of aligned PLA, collagen, and coaxial scaffolds (6 mm in diameter, 0.125×10^6 cells per disc) in the serum-free ITS+ medium (Sigma-Aldrich) supplemented with 10 ng/mL TGFβ1 (PeproTech) for 2 weeks with medium changes every 3–4 days. The scaffold and cells were solubilized with pepsin under acidic conditions and digested with pancreatic elastase at neutral pH to convert polymeric collagen to monomeric collagen at 2–8°C. To evaluate newly deposited collagen, an enzyme-linked immunosorbent assay (ELISA) was performed (Human collagen type I ELISA; MD Bioproducts). The plate was read on a SpectraMax 384 Plate Reader (Molecular Devices) at 450 nm (650 nm reference). Nonspecific ELISA readings were controlled by using noncell-seeded scaffolds cultured under the same conditions and times.

Biochemical assays

Biochemical assays were performed on PLA, collagen, and coaxial constructs with or without cells cultured for 2 weeks. Constructs ($n=5$) were digested papain (construct/1 mL papainase solution; 125 μg/mL) in 0.1 M sodium acetate, 5 mM cysteine HCl, and 0.05M EDTA (pH 6.0) (all from Sigma-Aldrich) at 60°C under constant rotation for 3 h. Total DNA content of constructs was quantified using the Quant-iT™ PicoGreen® dsDNA Reagent and Kits (Invitrogen, Carlsbad, CA). Proteoglycan content was estimated by quantifying the amount of sulfated glycosaminoglycan (sGAG) in constructs using the dimethylmethylene blue dye-binding assay (Blyscan; Biocolor Ltd., Carrickfergus, United Kingdom) with a chondroitin sulfate standard.

RNA isolation and reverse-transcription polymerase chain reaction

Total RNA was isolated using the RNeasy Mini Kit (Qiagen, Hilden, Germany) and first-strand cDNA was made as per the manufacturer's protocol (Applied Biosystems, Foster City, CA). Quantitative reverse transcription–polymerase chain reaction was performed using TaqMan® gene expression reagents. *COL1A1*, *ACAN*, *SOX9*, *COMP*, *THY-1*, *CHAD*, *TNC*, *SCX*, and *GAPDH* were detected using Assays-on-Demand™ primer/probe sets (Applied Biosystems). Expression levels were normalized to *GAPDH* using the recommended ΔCt method, and fold change was calculated using the $2^{-\Delta\Delta CT}$ formula.[27]

Ex vivo *meniscal repair*

Meniscal tissue from the avascular zone was harvested from fresh, young bovine knees and cut into rectangular sections (width: 12.25 ± 0.42 mm, length: 15.98 ± 1.45 mm, and thickness: 2.37 ± 0.32 mm) and were cultured in medium for 5 days in six-well plates with DMEM supplemented with 10% calf serum and 1% Penicillin–Streptomycin–Glutamine. A longitudinal meniscal tear (nominally 10 mm in length) was surgically created (with a scalpel) parallel to the circumferential direction of the collagen bundles. Scaffolds were seeded with avascular human meniscal cells, were cultured for 2 weeks, and then were inserted in the meniscal tear with the scaffold fibers aligned parallel to the circumferential fibers of the host meniscal tissue. The repaired meniscal explants were maintained in serum-free ITS+ medium (Sigma-Aldrich) supplemented with 10 ng mL^{-1} TGFβ1 (PeproTech) (8 mL $well^{-1}$) for an additional 3 weeks (with medium changes every 4–5 days).

Histology and immunohistochemistry

Ex vivo meniscal explants with tears repaired with cell-seeded or acellular scaffolds were fixed in Z-Fix (ANATECH, Battle Creek, MI) for 7 days and embedded in paraffin. Sections (5–7 μm thick) were stained with Hematoxylin and Eosin for morphological analysis and with Safranin O–Fast Green staining to assess glycosaminoglycan (GAG) distribution. For detection of collagen type I by immunohistochemistry (IHC), cut sections were treated with hyaluronidase for 2 h[28] and were incubated overnight at 4°C with a primary antibody against collagen type I (clone: I-8H5; MP Biomedicals, Santa Ana, CA) at 10 μg mL^{-1}.

Secondary antibody staining and detection procedures were followed as previously described.[9,26] An isotype control was used to monitor nonspecific staining. To count cells, sections were stained with VECTASHIELD® mounting medium containing 4′,6-diamidino-2-phenylindole (DAPI; Vector Laboratories, Burlingame, CA).

Mechanical testing of meniscal repairs

Bovine meniscus explants with untreated tears or with tears repaired with cell-seeded or acellular scaffolds ($n=8$ per group) were tested as previously described.[9] After 3 weeks in culture, the specimens were moved into 50-mL conical tubes and were washed with 1×PBS. The ends of the specimen were mounted in the clamps of an Instron mechanical testing frame (Instron Universal Testing Machine, 3342 Single Column Model, Instron). Tensile force was monitored as the samples were tested to failure in tension at a constant displacement rate of 1 mm s^{-1}. Tensile modulus was calculated from the slope of the linear segment of the stress–strain curve. UTS was calculated at the maximum load before failure.

Statistical analysis

Kruskal–Wallis and Mann–Whitney tests were used to detect statistically significant differences in fiber diameter, mechanical properties, and gene expression between scaffold types. Also, groups of different cultured scaffolds with or without cells for the mechanical properties and groups of different cultured scaffolds with either no growth or TGFβ1 factor for gene expression were compared by two-way analysis of variance (ANOVA). *p*-Values less than 0.05 were considered statistically significant.

Results

Ultrastructure of core–shell fibers

TEM (Fig. 1C) revealed the core–shell structure of each fiber, with the darker core of PLA. The collagen shell in individual nanofibers had an average thickness of 61.55 ± 7.06 nm. Electrospinning onto a spinning drum generated scaffold structures with a high degree of alignment (Fig. 1D, E). The average diameter of noncrosslinked fibers was 0.24 ± 0.012 μm (range, 0.14–0.31 μm) and that for crosslinked fibers was 0.32 ± 0.016 μm (range, 0.2–0.38 μm). The thickness of noncrosslinked scaffolds was 0.21 ± 0.04 mm, whereas crosslinked scaffolds were 0.19 ± 0.03 mm. SEM images of noncrosslinked and crosslinked samples, after exposure to culture medium, demonstrate the degradation of the uncrosslinked collagen in Figures 1F and G.

TGA and FTIR of PLA, collagen, and coaxial scaffolds

The thermal stability of the different electrospun scaffolds was analyzed, and the results are shown in Figure 2A. The onset of degradation of collagen scaffolds (292°C) was earlier than that of PLA scaffolds (318°C); whereas the coaxial scaffolds exhibited an intermediate onset of degradation at 305°C. Furthermore, the residual mass obtained at 500°C was 0, 50, and 23.5 wt% in PLA, collagen, and coaxial scaffolds, respectively, supporting the collagen content expected in coaxial electrospun scaffolds.

Figure 2B shows the FTIR spectra of PLA, collagen, and coaxial electrospun samples. The absorption bands in collagen represent the characteristic amide I at about 1650–1660 cm^{-1}, which is due to stretching vibrations of peptide C=O groups, amide II in the range of 1540–1555 cm^{-1}, originating from stretching C-N and bending N-H, and a broad and middle amide A at about 3300–3600 cm^{-1} due to N-H stretch in resonance with amide II overtone.[29,30] PLA scaffolds do not have any strong peak in the 1540–1660 cm^{-1} region (amide I and amide II peaks). However, coaxial scaffolds show the peaks of amide I and II as well as slightly amide A.

Hydrophilicity of PLA, collagen, and coaxial scaffolds

The hydrophilicity of the scaffold surfaces was measured using the water droplet contact angle (Fig. 3A). As

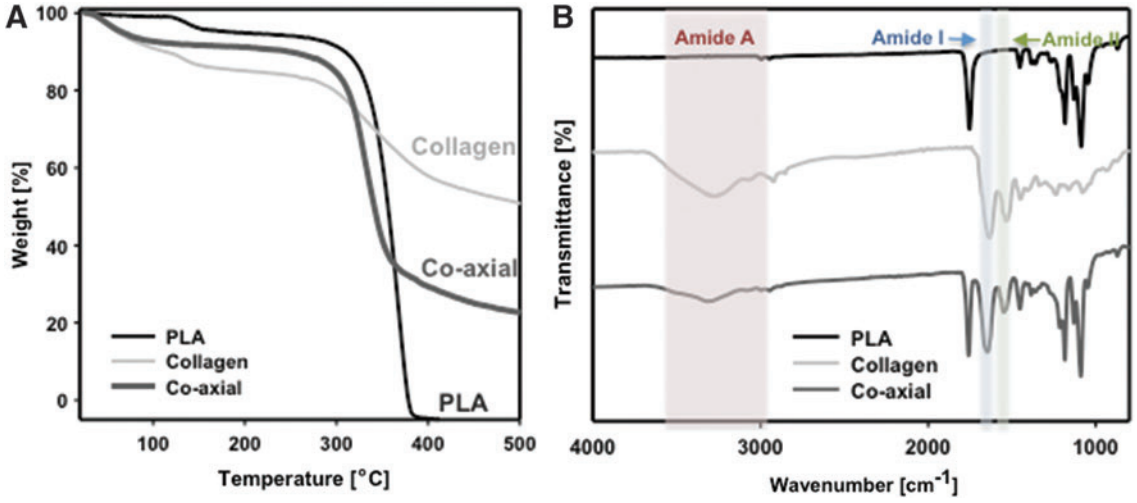

FIG. 2. Characterizations of different electrospun scaffolds. **(A)** Thermogravimetric analysis and **(B)** FTIR spectra of three different electrospun scaffolds, PLA, collagen, and coaxial electrospun scaffolds. FTIR, Fourier transform infrared. Color images are available online.

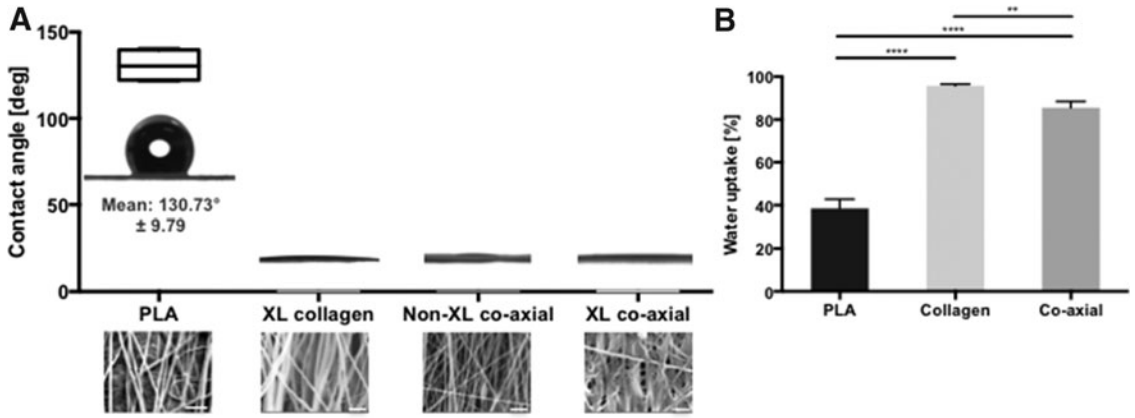

FIG. 3. Hydrophilic property of coaxial electrospun scaffolds. **(A)** Water droplet profiles and the graph of the contact angles of 1 μL drops of water on PLA, crosslinked (XL) collagen, noncrosslinked (non-XL) coaxial, and crosslinked (XL) coaxial scaffold with *insets* of SEM image of each scaffold (PLA: 2500×, scale bar: 10 μm; others: 10,000×, scale bar: 2 μm) of scaffolds. **(B)** Percentage of water uptake by PLA, collagen, and coaxial scaffolds. ($p = 0.0019$ among experimental groups, Kruskal–Wallis test; $^{**}p < 0.01$ and $^{****}p < 0.0001$ between groups, Mann–Whitney test).

expected, PLA scaffolds were hydrophobic with a contact angle averaging 131°. Coaxial electrospun scaffolds were highly hydrophilic. The water droplet disappeared when placed on noncrosslinked collagen. On crosslinked scaffolds, the droplet contact angle approached 0°. Water content also was significantly increased in coaxial electrospun scaffolds (Fig. 3B).

Mechanical properties of electrospun scaffolds

Dry PLA and coaxial electrospun scaffolds had significantly higher average tensile modulus (Fig. 4A, 347 ± 36 MPa; and 376 ± 47 MPa, respectively) compared with collagen scaffolds (179 ± 79 MPa; Mann–Whitney test, $p < 0.0001$). The UTS of PLA (15 ± 0.68 MPa) and coaxial electrospun

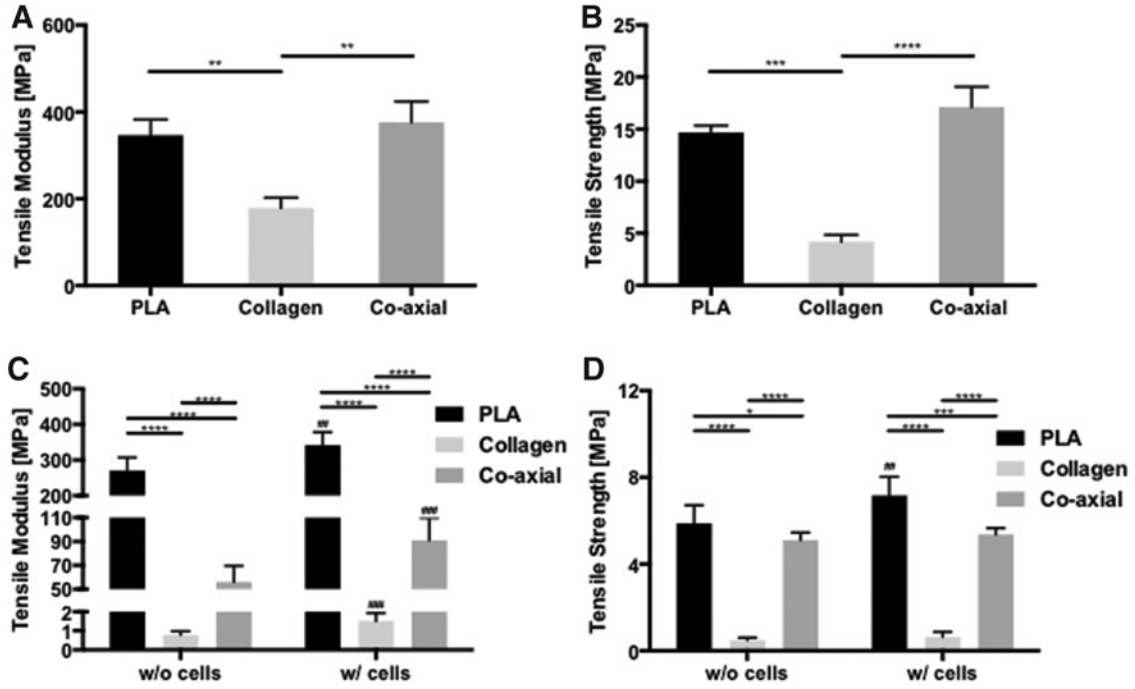

FIG. 4. Mechanical properties of different electrospun scaffolds and cell-seeded scaffolds. **(A)** Tensile modulus ($p = 0.0038$ among experimental groups, Kruskal–Wallis test; $^{**}p < 0.01$ between groups, Mann–Whitney test), and **(B)** UTS ($p = 0.0003$ among experimental groups, Kruskal–Wallis test; $^{***}p < 0.001$ and $^{****}p < 0.0001$ between groups, Mann–Whitney test) for dry PLA, collagen, and coaxial scaffolds. **(C)** Tensile modulus ($p = 0.0004$ for interaction, $p < 0.0001$ for the existence of cells, and $p < 0.0001$ among experimental groups, two-way ANOVA) and **(D)** UTS ($p = 0.0076$ for interaction, $p = 0.0008$ for the existence of cells, and $p < 0.0001$ among experimental groups, two-way ANOVA; Bar+ $^{*}p < 0.05$, Bar+ $^{***}p < 0.001$, and Bar+ $^{****}p < 0.0001$ between groups, Mann–Whitney test; $^{\#\#}p < 0.01$, and $^{\#\#\#}p < 0.001$ acellular versus cellular scaffolds in the same type of scaffolds, Mann–Whitney test) of electrospun PLA, collagen, and coaxial scaffolds in culture with or without cells for 2 weeks. ANOVA, analysis of variance; UTS, ultimate tensile strength.

(17 ± 1.95 MPa) scaffolds was also significantly higher than that of collagen scaffolds (4.2 ± 0.66 MPa, Mann–Whitney test, $p < 0.0001$) (Fig. 4B).

The mechanical properties of all scaffolds were reduced after culture (Fig. 4C, D). However, PLA and coaxial electrospun scaffolds maintained relatively greater mechanical properties than collagen scaffolds. In terms of loss of mechanical property, wet collagen scaffolds without cells had 99.57% decreased tensile modulus compared with dry collagen scaffolds, whereas wet coaxial scaffolds without cells had 85.10% loss of tensile modulus in comparison to dry coaxial scaffolds. Otherwise, PLA had only 21.88% loss of tensile modulus. Cell seeding also had a significant effect, increasing the stiffness and tensile strength significantly in all scaffolds compared with each acellular scaffold (Fig. 4C, D).

Cell viability

Human meniscal avascular cells seeded on noncrosslinked coaxial scaffolds attached only to some areas, presumably due to loss of the collagen coating (Fig. 5A). Cells seeded on crosslinked coaxial electrospun scaffolds attached to the entire surface and appeared elongated in the direction of the fibers (Fig. 5B). These differences in cell attachment, morphology, and alignment were also reflected in the confocal images (Fig. 5C, D), which provided evidence of high cell viability in the scaffolds. Figure 5E and F show cell viability of avascular cells on PLA and collagen-aligned scaffolds for 2 weeks in culture with same media as the cell viability of cells on the coaxial scaffolds. Biochemical analyses indicated similar cellularity in collagen and coaxial scaffolds and extracellular matrix comprised of proteoglycans and collagens (Fig. 6A–C). Greater amounts of GAG and collagen were observed in both collagen and coaxial scaffolds compared with PLA scaffolds.

Meniscogenic gene expression

We measured gene expression of *COL1A1*, *COL2A1*, *COMP*, and *ACAN* for matrix proteins; *SOX9*, *THY-1*, and *CHAD* for mesenchymal differentiation; and *TNC* and *SCX* for meniscal growth and development (but *COL2A1* did not detect) as previously described.[26] Cells cultured on PLA,

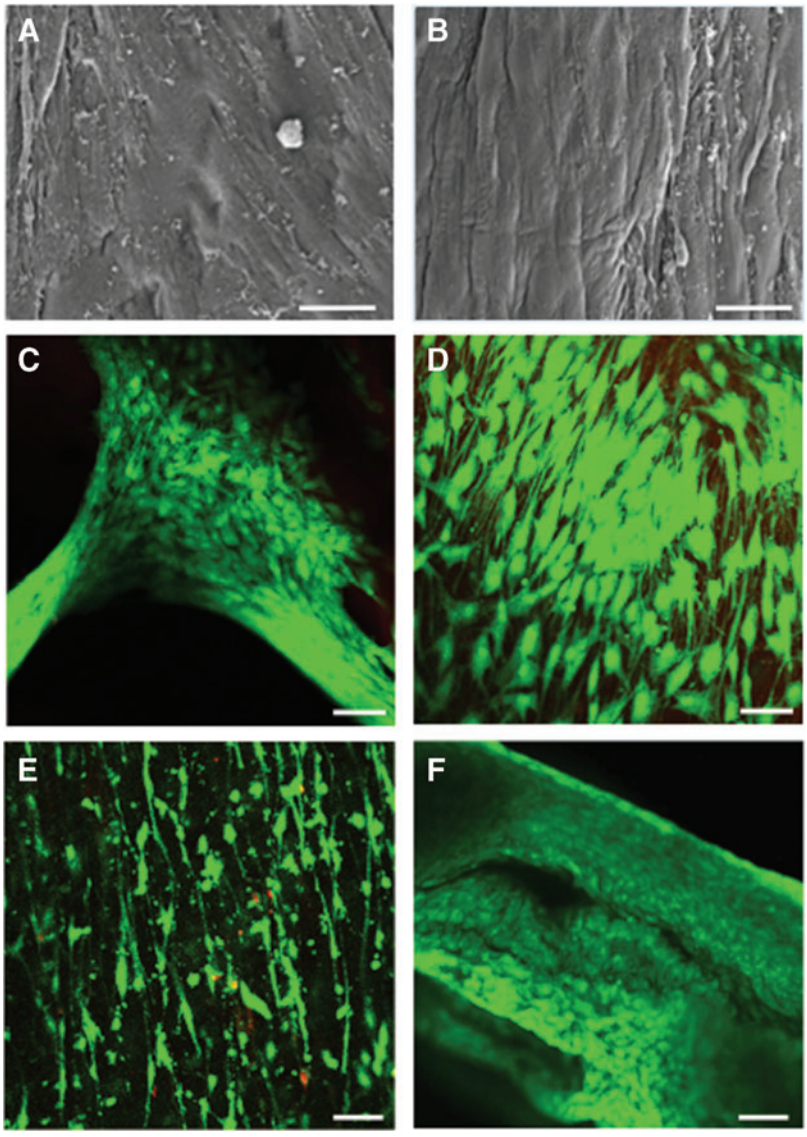

FIG. 5. Cellular morphology, and cell viability on scaffolds. Cellular morphology, and cell viability on scaffolds. SEM (Mag.: 625×; scale bar: 20 μm) of human meniscus cells seeded on **(A)** noncrosslinked; and **(B)** crosslinked coaxial scaffolds. Viability of human meniscus cells cultivated on **(C)** noncrosslinked coaxial scaffold, **(D)** crosslinked coaxial scaffold, **(E)** PLA scaffold, and **(F)** collagen scaffold (Mag.: 10×; scale bar: 200 μm in confocal images). Color images are available online.

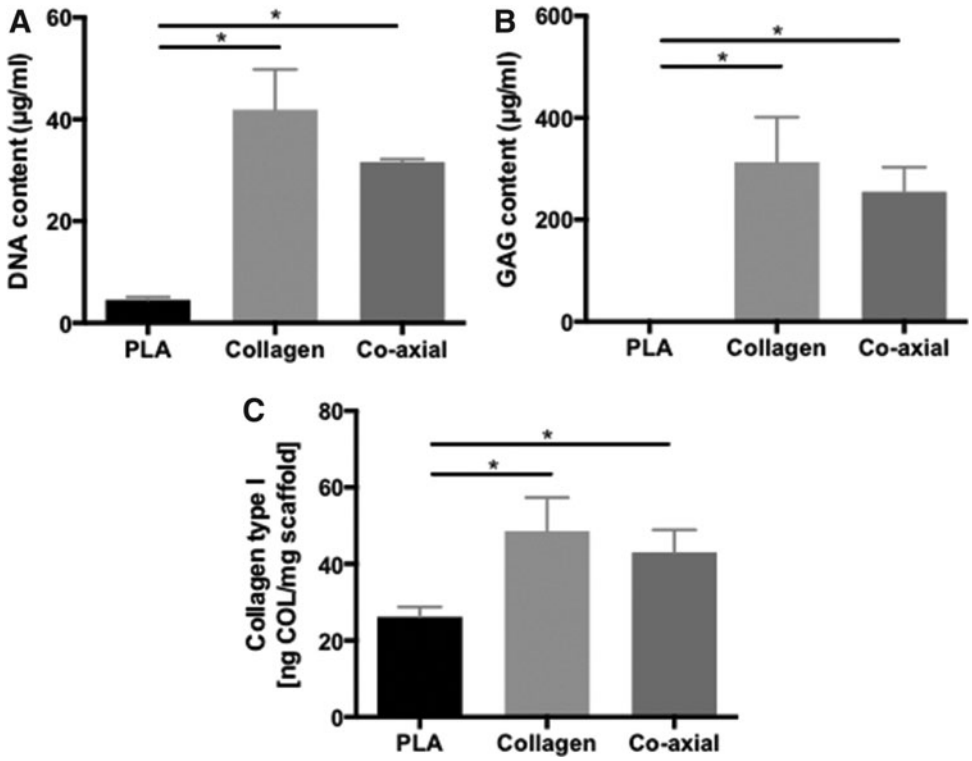

FIG. 6. Matrix protein and DNA quantifications of different electrospun scaffolds with cells. **(A)** DNA assay, **(B)** GAG assay, and **(C)** Collagen type I assay of electrospun PLA, collagen, and coaxial scaffolds in culture with cells for 2 weeks. ($p < 0.0001$ among experimental groups Kruskal–Wallis test; Bar+ $*p < 0.05$ between groups, Mann–Whitney test). GAG, glycosaminoglycan.

collagen, and coaxial electrospun scaffolds expressed significantly higher levels of *COL1A1*, *ACAN*, *SOX9*, *COMP*, *THY-1*, *CHAD*, *TNC*, and *SCX* genes relative to monolayer-cultured cells (Fig. 7, Kruskal–Wallis test and two-way ANOVA, $p < 0.05$). Cells on collagen and coaxial electrospun scaffolds expressed more *COLA1*, *ACAN*, *COMP*, *CHAD*, *TNC*, and *SCX* than cells on PLA scaffolds, especially in the presence of TGFβ1.

Repair of ex vivo *meniscal tears*

After 3 weeks of postrepair culture, no repair tissue was found in untreated control tears (Fig. 8A). Acellular coaxial electrospun scaffolds filled the tear but without any evidence of cellular infiltration (Fig. 8B). On the other hand, cell-seeded coaxial electrospun scaffolds generated newly formed tissue that filled the tear and appeared histologically integrated with the host tissue (Fig. 8C). The repair tissue consisted of cells with elongated morphology, collagen type I positive matrix staining (IHC), and evidence of scaffold/neotissue integration within the defect.

On mechanical testing of the repaired explants, preparation of specimens is shown in Figure 9A and cell-seeded scaffolds ($n = 8$) generated significantly greater tensile mechanical properties (tensile modulus $= 3.00 \pm 0.36$ MPa and UTS $= 0.89 \pm 0.07$ MPa) compared with either unrepaired defects (tensile modulus $= 0.61 \pm 0.07$ MPa, Mann–Whitney test, $p = 0.0019$ and UTS $= 0.51 \pm 0.06$ MPa, Mann–Whitney test, $p = 0.0002$) or defects repaired with acellular scaffolds (tensile modulus $= 1.09 \pm 0.12$ MPa, Mann–Whitney test, $p = 0.0002$, and UTS $= 0.56 \pm 0.05$ MPa, Mann–Whitney test, $p = 0.0011$) (Fig. 9B, C). The differences across all three groups were statistically significant (Kruskal–Wallis test; $p = 0.0021$ for UTS; $p < 0.0001$ for tensile modulus).

Discussion

The success of a cell-based tissue-engineered meniscus graft relies on its ability to mimic native three-dimensional microstructure, to support cell growth and function to produce tissue-specific matrix, and to enhance graft integration into the repair site. We had previously shown proof of concept of engineering meniscogenic tissue by electrospinning PLA and collagen type I.[8,9] While PLA scaffolds possessed the desired mechanical properties, collagen scaffolds induced better cell attachment and enhanced meniscogenic tissue formation. Coaxial electrospinning, first demonstrated by Sun *et al.*,[15] is a dynamic process that generates nanofibers in a core–shell configuration. By modulating the feed rate of the inner and outer polymer solutions, we fabricated nanofibrous scaffolds that combined the properties of two biomaterials to more closely emulate the structure, mechanical properties, and biochemical composition of native meniscal tissue.[15,31] The SEM images of our electrospun mats resemble published reports of SEM of native human menisci.[32,33] The coaxial electrospun scaffolds supported the viability of human meniscus cells, induced an organized cellular alignment reflecting the underlying meniscal microstructure, and enhanced the formation of meniscus-like tissues, compared with noncoaxial electrospun scaffolds of each individual polymer. The potential for the repair of meniscal tears was demonstrated by the formation and integration of new tissue in *ex vivo* meniscal tears.

Coaxial scaffolds have simultaneously higher mechanical properties and water uptake capacities

The morphology and hydrophilic/hydrophobic qualities of the scaffolds affected the rate of water uptake of the scaffolds and influenced subsequent cell response.[34–36] We

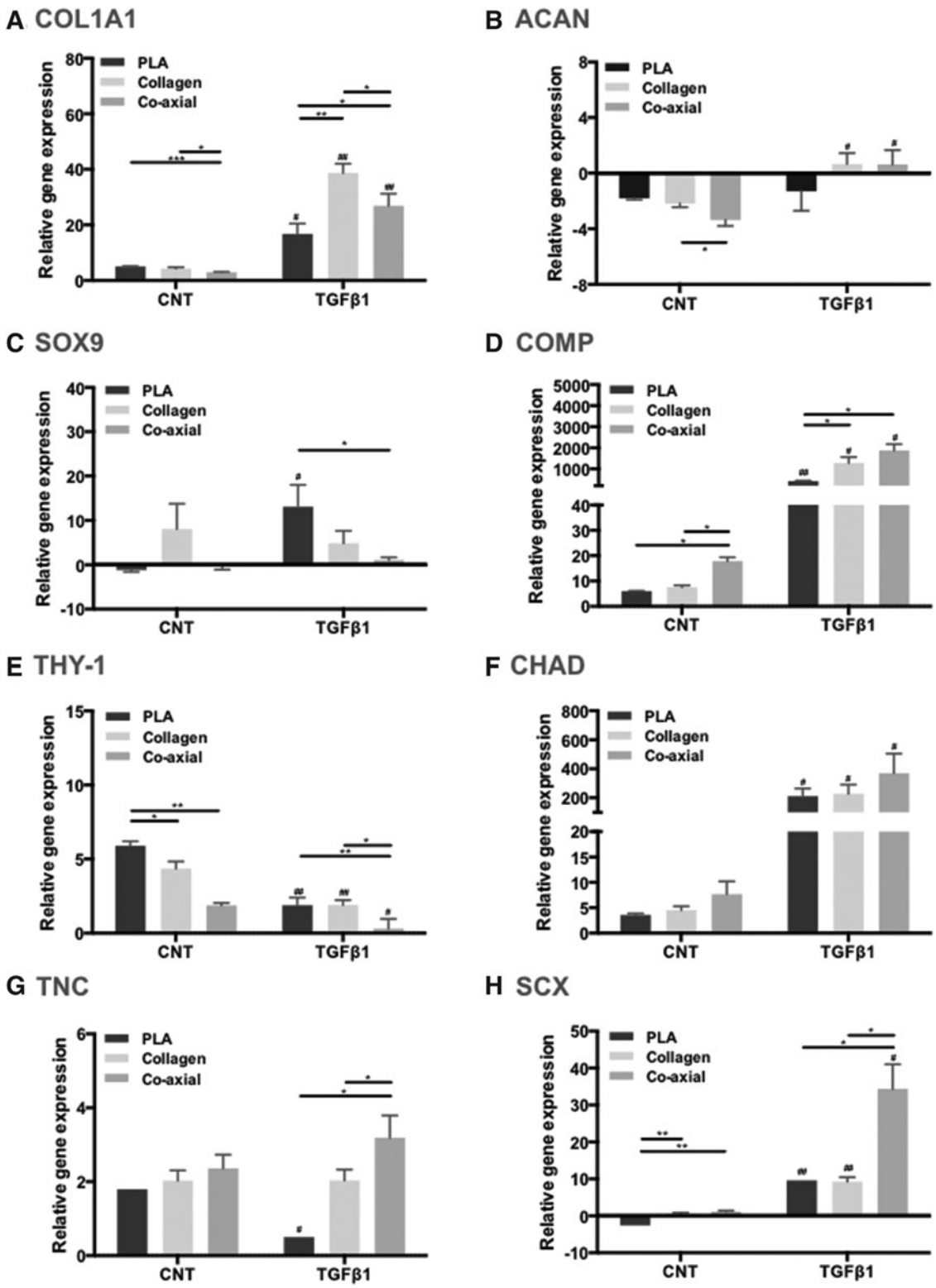

FIG. 7. Gene expression of human meniscus cells cultured on PLA, collagen, and coaxial scaffolds. **(A)** *COL1A1*; **(B)** *ACAN*; **(C)** *SOX9*; **(D)** *COMP*; **(E)** *THY-1*; **(F)** *CHAD*; **(G)** *TNC*; and **(H)** *SCX*. Gene expression is relative to cells cultured under monolayer conditions. ($p < 0.05$ among experimental groups, two-way ANOVA; and Bar+ $^{*}p < 0.05$, Bar+ $^{**}p < 0.01$, and Bar+ $^{***}p < 0.001$ between groups, Mann–Whitney test; $^{\#}p < 0.05$ and $^{\#\#}p < 0.01$, CNT versus TGFβ1 in the same type of scaffolds, Mann–Whitney test).

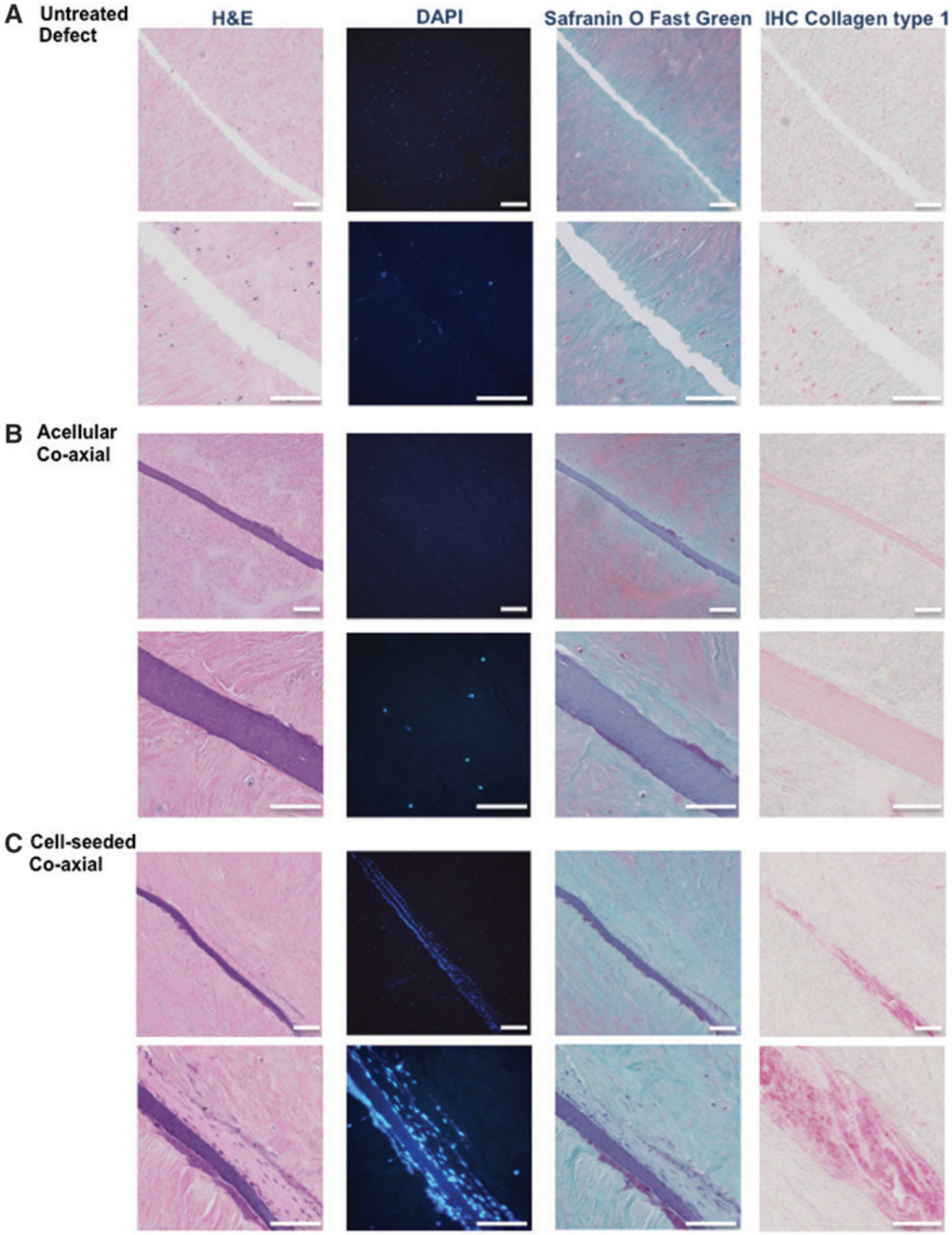

FIG. 8. Representative histological images of *ex vivo* repair: Hematoxylin and Eosin, DAPI, Safranin O/fast green, and collagen type I immunostaining. **(A)** untreated tear. Surgically created tears implanted with **(B)** acellular coaxial scaffolds: or **(C)** cell-seeded coaxial scaffolds (Low Mag.: 10×; scale bar: 200 μm; High Mag.: 40×; scale bar: 100 μm). All constructs were cultured for 3 weeks and then processed for histology. DAPI, 4′,6-diamidino-2-phenylindole. Color images are available online.

have previously reported better attachment of cells seeded on collagen scaffolds with greater secretion of matrix proteins than cells seeded on PLA scaffolds.[9] Our present study provides evidence that coaxial electrospun scaffolds were significantly more hydrophilic than PLA-only scaffolds, based on water droplet contact angle measurement as well as water uptake abilities (Fig. 2A, B). Cells seeded on crosslinked coaxial scaffolds attached to the entire surface further supporting our hypothesis that a shell of collagen increases cell attachment. In contrast, cells seeded on noncrosslinked coaxial electrospun scaffolds only attached to some regions, presumably because of localized loss of the uncrosslinked

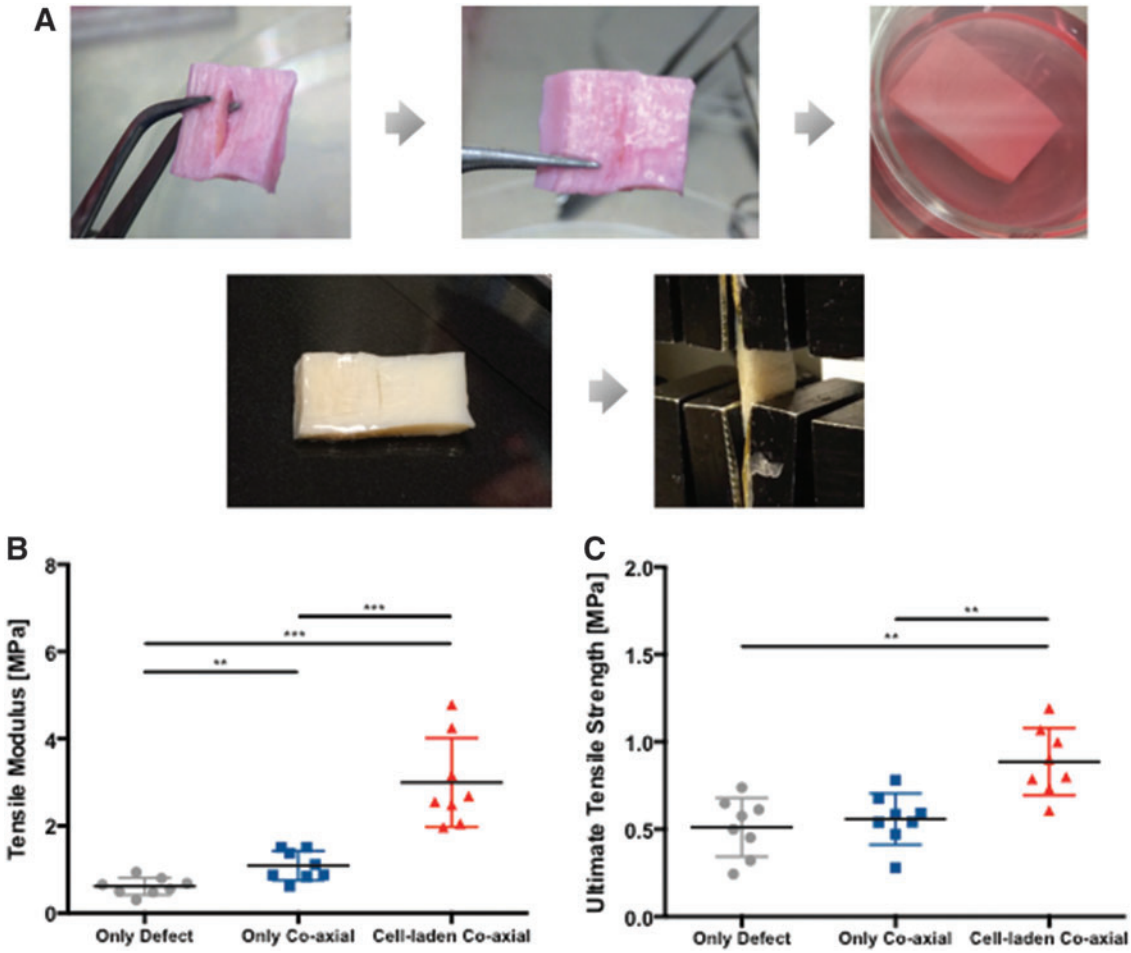

FIG. 9. Mechanical strength of meniscus *ex vivo* repair. **(A)** Photographs the meniscus explant with surgically created tear, scaffold implantation, culturing, and tensile testing. **(B)** Tensile modulus ($p < 0.0001$ among experimental groups, Kruskal–Wallis test) and **(C)** UTS ($p = 0.0021$ among experimental groups, Kruskal–Wallis test; $^{**}p < 0.01$ and $^{***}p < 0.001$ between groups, Mann–Whitney test) of meniscal tears repaired with cell-seeded coaxial scaffolds compared with untreated tears and tears repaired with acellular coaxial scaffolds. Color images are available online.

collagen as it dissolved into the culture medium. The higher levels of meniscogenic gene expression in cells cultured on collagen and coaxial electrospun scaffolds, supports the importance of scaffold hydrophilicity in modulating the generation of meniscus-like tissues.

Dry collagen scaffolds have high mechanical properties that degrade quickly as the scaffolds are hydrated in culture or after implantation. While some studies have reported high mechanical properties with dry scaffolds,[37] the performance after hydration is more clinically relevant. The bending modulus of individual electrospun collagen fibers reduces precipitously from over 1 GPa to 0.07–0.26 MPa after hydration in the saline buffer.[10] In our study, the tensile modulus of dry collagen-only scaffolds dropped from 179 MPa to less than 1 MPa after culture. On the other hand, coaxial electrospun scaffolds retained much of their mechanical properties, even after culture, which supports our primary hypothesis that coaxial electrospinning can combine the advantages of PLA and collagen. Our coaxial electrospun scaffolds had higher tensile mechanical properties than previously reported for polymer scaffolds that combined synthetic materials and natural proteins. For example, Kai *et al.*[38] measured tensile properties of blended and coaxial PCL/gelatin electrospun nanofibers. After hydration for 3 h, the tensile modulus was only 0.13 ± 0.04 MPa for the blended scaffolds and 0.56 ± 0.09 MPa for the coaxial scaffolds. Similarly, Lee *et al.*[39] reported on PCL/collagen composite electrospun scaffolds with a tensile modulus of only 2.7 ± 1.2 MPa. The tensile mechanical properties of our coaxial electrospun scaffolds (Fig. 4) were comparable to those reported for human meniscus ranging from 43 to 160 MPa.[40–42]

Coaxial scaffolds encourage meniscogenic differentiation for meniscus regeneration

Functionalizing the core of PLA with a sheath of collagen enhanced the meniscogenic response in cells reflected by the increased gene expression (*COLA1*, *ACAN*, *COMP*, *CHAD*, *TNC*, and *SCX*) relative to noncoaxial scaffolds of PLA. This gene expression was supported by the IHC for collagen 1 (the dominant protein in meniscal tissue) in the neotissue formed during repair of *ex vivo* meniscal tears. Some expression of *ACAN* was also expected because the avascular zone of the normal meniscus was often

proteoglycan-containing regions. We have shown *COMP* and *CHAD* to be important genes in defining the differentiated meniscal phenotype.[43] *TNC* and *SCX* have also been implicated in meniscus development.[44–48] In contrast, *THY-1*, a marker of dedifferentiation, was downregulated on coaxial electrospun scaffolds.

Cell seeding significantly increased mechanical properties. After 2 weeks in culture, the tensile modulus of cell-seeded coaxial electrospun scaffolds increased by 62.27% compared with the acellular scaffolds. The tensile modulus of cell-seeded PLA-only scaffolds increased by 26.24% relative to acellular PLA scaffolds. This greater relative difference in mechanical properties between cell-seeded and acellular coaxial electrospun scaffolds was likely due to more newly regenerated extracellular matrix, as supported by cell viability, gene expression, and histology.

Coaxial scaffolds can repair ex vivo *tears in avascular meniscus*

We had previously developed and characterized an *ex vivo* model to study the repair of meniscal tears.[9] The repair in meniscal tissue explants provides proof of concept of potential treatment of tears in the avascular zone. In the present study, the cellular response and histological integration between electrospun scaffold and host tissue were promising. We also tested the mechanical strength of the biomechanical integration after *ex vivo* implantation into the tear. Repairing the meniscal tear with cell-seeded coaxial electrospun scaffolds not only resulted in significant new collagen I deposition, but also enhanced integration into the host tissue, which was reflected in the increased mechanical strength.

Limitations

Despite the promising interaction of human meniscus cells with the coaxial electrospun scaffolds and the encouraging new tissue formation, several issues remain to be addressed for a successful application to enhance meniscal tissue repair. Since the menisci are fibrocartilaginous crescent-shaped tissue, we are developing fiber collectors to generate the shapes and sizes representative of human menisci. Human meniscal cells are not easily harvested clinically for autologous use. We are also exploring alternative cell sources, such as synovial cells or cells from the infrapatellar fat pad, which are more clinically relevant for autologous applications, and embryonic stem cells as an allogeneic source.[26] While our primary intention in the present study was to demonstrate proof of concept with respect to biocompatibility and biomechanical property of coaxial scaffolds, meniscal cell phenotype, and neotissue formation, in future studies we aim to test whether these constructs can be used to repair defects created in an *in vivo* model.

Conclusions

We electrospun coaxial scaffolds to generate scaffolds with the mechanical strength of PLA and the biocompatibility of collagen. Coaxial electrospun scaffolds induced greater meniscogenic gene expression than PLA-alone scaffolds and generated repair tissue that integrated well into *ex vivo* meniscal tears. Coaxial electrospun scaffolds may therefore have potential for meniscal tissue engineering.

Acknowledgments

Funding was provided by the National Institutes of Health (P01 AG007996), by the Shaffer Family Foundation, and by Donald and Darlene Shiley. The authors are grateful to Judy Blake for the efforts (copyediting).

Authors' Contributions

J.B., M.K.L., and D.D.D. designed the study and wrote the article. J.B. conducted cell culture studies and conducted histology and qualitative polymerase chain reaction analyses. J.B. conducted and interpreted the SEM analysis. J.B. conducted the *ex vivo* repair model. All authors discussed the results and approved the final version of the article.

Disclosure Statement

No competing financial interests exist.

References

1. Englund, M., Roemer, F.W., Hayashi, D., Crema, M.D., and Guermazi, A. Meniscus pathology, osteoarthritis and the treatment controversy. Nat Rev Rheumatol **8,** 412, 2012.
2. Garrett, W.E., Jr., Swiontkowski, M.F., Weinstein, J.N., *et al.* American board of orthopaedic surgery practice of the orthopaedic surgeon: Part-II, certification examination case mix. J Bone Joint Surg **88,** 660, 2006.
3. Nepple, J.J., Dunn, W.F., and Wright, R.W. Meniscal repair outcomes at greater than five years: a systematic literature review and meta-analysis. J Bone Joint Surg **94,** 2222, 2012.
4. Whitehouse, M.R., Howells, N.R., Parry, M.C., *et al.* Repair of torn avascular meniscal cartilage using undifferentiated autologous mesenchymal stem cells: from in vitro optimization to a first-in-human study. Stem Cells Transl Med **6,** 1237, 2017.
5. Mauck, R.L., and Burdick, J.A. From repair to regeneration: biomaterials to reprogram the meniscus wound microenvironment. Ann Biomed Eng **43,** 529, 2015.
6. Makris, E.A., Hadidi, P., and Athanasiou, K.A. The knee meniscus: structure-function, pathophysiology, current repair techniques, and prospects for regeneration. Biomaterials **32,** 7411, 2011.
7. Petersen, W., and Tillmann, B. Collagenous fibril texture of the human knee joint menisci. Anat Embryol (Berl) **197,** 317, 1998.
8. Baek, J., Chen, X., Sovani, S., Jin, S., Grogan, S.P., and D'Lima, D.D. Meniscus tissue engineering using a novel combination of electrospun scaffolds and human meniscus cells embedded within an extracellular matrix hydrogel. J Orthop Res **33,** 572, 2015.
9. Baek, J., Sovani, S., Glembotski, N.E., *et al.* Repair of avascular meniscus tears with electrospun collagen scaffolds seeded with human cells. Tissue Eng Part A **22,** 436, 2016.
10. Yang, L., Fitié, C.F., van der Werf, K.O., Bennink, M.L., Dijkstra, P.J., and Feijen, J. Mechanical properties of

single electrospun collagen type I fibers. Biomaterials **29,** 955, 2008.
11. O'Brien, F.J. Biomaterials & scaffolds for tissue engineering. Mater Today **14,** 88, 2011.
12. Wang, Y.-F., Guo, H.-F., and Ying, D.-J. Multilayer scaffold of electrospun PLA–PCL–collagen nanofibers as a dural substitute. J Biomed Mater Res B Appl Biomater **101,** 1359, 2013.
13. Hall Barrientos, I.J., Paladino, E., Szabó, P., *et al.* Electrospun collagen-based nanofibres: a sustainable material for improved antibiotic utilisation in tissue engineering applications. Int J Pharm **531,** 67, 2017.
14. Loscertales, I.G., Barrero, A., Guerrero, I., Cortijo, R., Marquez, M., and Gañán-Calvo, A.M. Micro/nano encapsulation via electrified coaxial liquid jets. Science **295,** 1695, 2002.
15. Sun, Z., Zussman, E., Yarin, A.L., Wendorff, J.H., and Greiner, A. Compound core–shell polymer nanofibers by co-electrospinning. Adv Mater **15,** 1929, 2003.
16. Yang, Y., Li, X., Qi, M., Zhou, S., and Weng, J. Release pattern and structural integrity of lysozyme encapsulated in core–sheath structured poly(dl-lactide) ultrafine fibers prepared by emulsion electrospinning. Eur J Pharm Biopharm **69,** 106, 2008.
17. Yang, Y., Xia, T., Zhi, W., *et al.* Promotion of skin regeneration in diabetic rats by electrospun core-sheath fibers loaded with basic fibroblast growth factor. Biomaterials **32,** 4243, 2011.
18. Kayaci, F., Ozgit-Akgun, C., Donmez, I., Biyikli, N., and Uyar, T. Polymer–inorganic core–shell nanofibers by electrospinning and atomic layer deposition: flexible nylon–ZnO core–shell nanofiber mats and their photocatalytic activity. ACS Appl Mater Interfaces **4,** 6185, 2012.
19. Peng, Q., Sun, X.-Y., Spagnola, J.C., Hyde, G.K., Spontak, R.J., and Parsons, G.N. Atomic layer deposition on electrospun polymer fibers as a direct route to Al2O3 microtubes with precise wall thickness control. Nano Lett **7,** 719, 2007.
20. Li, Z., Huang, H., and Wang, C. Electrostatic forces inducepoly(vinyl alcohol)-protected copper nanoparticles toform copper/poly(vinyl alcohol) nanocables via electrospinning. Macromol Rapid Commun **27,** 152, 2006.
21. Pant, H.R., Risal, P., Park, C.H., Tijing, L.D., Jeong, Y.J., and Kim, C.S. Core–shell structured electrospun biomimetic composite nanofibers of calcium lactate/nylon-6 for tissue engineering. Chem Eng J **221,** 90, 2013.
22. Fakhrali, A., Ebadi, S.V., and Gharehaghaji, A.A. Production of core-sheath nanofiber yarn using two opposite asymmetric nozzles. Fiber Polym **15,** 2535, 2014.
23. Lee, B.-S., Jeon, S.-Y., Park, H., Lee, G., Yang, H.-S., and Yu, W.-R. New electrospinning nozzle to reduce jet instability and its application to manufacture of multi-layered nanofibers. Sci Rep **4,** 6758, 2014.
24. Liu, J., Shen, Z.H., Lee, S.H., Marquez, M., and McHugh, M.A. Electrospinning in compressed carbon dioxide: hollow or open-cell fiber formation with a single nozzle configuration. J Supercrit Fluids **53,** 142, 2010.
25. Pauli, C., Grogan, S.P., Patil, S., *et al.* Macroscopic and histopathologic analysis of human knee menisci in aging and osteoarthritis. Osteoarthritis Cartilage **19,** 1132, 2011.
26. Baek, J., Sovani, S., Choi, W., Jin, S., Grogan, S.P., and D'Lima, D.D. Meniscal tissue engineering using aligned collagen fibrous scaffolds: comparison of different human cell sources. Tissue Eng Part A **24,** 81, 2018.
27. Martin, I., Jakob, M., Schafer, D., Dick, W., Spagnoli, G., and Heberer, M. Quantitative analysis of gene expression in human articular cartilage from normal and osteoarthritic joints. Osteoarthritis Cartilage **9,** 112, 2001.
28. Roberts, S., Menage, J., Sandell, L.J., Evans, E.H., and Richardson, J.B. Immunohistochemical study of collagen types I and II and procollagen IIA in human cartilage repair tissue following autologous chondrocyte implantation. Knee **16,** 398, 2009.
29. Fiorani, A., Gualandi, C., Panseri, S., *et al.* Comparative performance of collagen nanofibers electrospun from different solvents and stabilized by different crosslinkers. J Mater Sci Mater Med **25,** 2313, 2014.
30. Sadeghi, A.R., Nokhasteh, S., Molavi, A.M., Khorsand-Ghayeni, M., Naderi-Meshkin, H., and Mahdizadeh, A. Surface modification of electrospun PLGA scaffold with collagen for bioengineered skin substitutes. Mater Sci Eng C **66,** 130, 2016.
31. Chakraborty, S., Liao, I.C., Adler, A., and Leong, K.W. Electrohydrodynamics: a facile technique to fabricate drug delivery systems. Adv Drug Deliv Rev **61,** 1043, 2009.
32. Villegas, D.F., and Donahue, T.L.H. Collagen morphology in human meniscal attachments: a SEM study. Connect Tissue Res **51,** 327, 2010.
33. Cui, J.H., and Min, B.-H. Collagenous fibril texture of the discoid lateral meniscus. Arthroscopy **23,** 635, 2007.
34. Arima, Y., and Iwata, H. Effect of wettability and surface functional groups on protein adsorption and cell adhesion using well-defined mixed self-assembled monolayers. Biomaterials **28,** 3074, 2007.
35. Miot, S., Woodfield, T., Daniels, A.U., *et al.* Effects of scaffold composition and architecture on human nasal chondrocyte redifferentiation and cartilaginous matrix deposition. Biomaterials **26,** 2479, 2005.
36. Mohan, N., Nair, P.D., and Tabata, Y. A 3D biodegradable protein based matrix for cartilage tissue engineering and stem cell differentiation to cartilage. J Mater Sci Mater Med **20,** 49, 2008.
37. Matthews, J.A., Wnek, G.E., Simpson, D.G., and Bowlin, G.L. Electrospinning of collagen nanofibers. Biomacromolecules **3,** 232, 2002.
38. Kai, D., Prabhakaran, M.P., Stahl, B., Eblenkamp, M., Wintermantel, E., and Ramakrishna, S. Mechanical properties and in vitro behavior of nanofiber-hydrogel composites for tissue engineering applications. Nanotechnology **23,** 095705, 2012.
39. Lee, S.J., Liu, J., Oh, S.H., Soker, S., Atala, A., and Yoo, J.J. Development of a composite vascular scaffolding system that withstands physiological vascular conditions. Biomaterials **29,** 2891, 2008.
40. Lechner, K., Hull, M.L., and Howell, S.M. Is the circumferential tensile modulus within a human medial meniscus affected by the test sample location and cross-sectional area? J Orthop Res **18,** 945, 2000.
41. Fithian, D.C., Kelly, M.A., and Mow, V.C. Material properties and structure-function relationships in the menisci. Clin Orthop Relat Res **252,** 19, 1990.
42. Tissakht, M., and Ahmed, A.M. Tensile stress-strain characteristics of the human meniscal material. J Biomech **28,** 411, 1995.
43. Grogan, S.P., Duffy, S.F., Pauli, C., Lotz, M.K., and D'Lima, D.D. Gene expression profiles of the meniscus avascular phenotype: a guide for meniscus tissue engineering. J Orthop Res **36,** 1947, 2018.

44. Koyama, E., Leatherman, J.L., Shimazu, A., Nah, H.-D., and Pacifici, M. Syndecan-3, tenascin-C, and the development of cartilaginous skeletal elements and joints in chick limbs. Dev Dyn **203,** 152, 1995.
45. Koyama, Y.-I., Norose, K., Kusubata, M., Irie, S., and Kusakabe, M. Differential expression of tenascin in the skin during hapten-induced dermatitis. Histochem Cell Biol **106,** 263, 1996.
46. Pacifici, M., Iwamoto, M., Golden, E.B., Leatherman, J.L., Lee, Y.-S., and Chuong, C.-M. Tenascin is associated with articular cartilage development. Dev Dyn **198,** 123, 1993.
47. Leal, M.F., Arliani, G.G., Astur, D.C., *et al.* Comprehensive selection of reference genes for expression studies in meniscus injury using quantitative real-time PCR. Gene **584,** 60, 2016.
48. Furumatsu, T., Kanazawa, T., Yokoyama, Y., Abe, N., and Ozaki, T. Inner meniscus cells maintain higher chondrogenic phenotype compared with outer meniscus cells. Connect Tissue Res **52,** 459, 2011.

Address correspondence to:
Darryl D. D'Lima, MD, PhD
Shiley Center for Orthopaedic Research and Education
Scripps Clinic
10666 North Torrey Pines Road, MS126
La Jolla, CA 92037

E-mail: ddlima@scripps.edu

Received: November 13, 2018
Accepted: March 13, 2019
Online Publication Date: August 14, 2019